Hydrogen and Oxygen Evolution in a Membrane Photoreactor Using Suspended Nanosized Au/TiO$_2$ and Au/CeO$_2$

Tiziana Marino [1],*, **Alberto Figoli** [1] , **Antonio Molino** [2] , **Pietro Argurio** [3] and **Raffaele Molinari** [3],*

[1] Institute on Membrane Technology (ITM), National Research Council of Italy (CNR), Via P. Bucci Cubo 17C, I-87036 Rende (CS), Italy; a.figoli@itm.cnr.it
[2] Research Centre of Portici, Italian National Agency for New Technologies, Energy and Sustainable Economic Development (ENEA), Piazzale Enrico Fermi 1, Portici, 80055 Napoli, Italy; antonio.molino@enea.it
[3] Department of Environmental and Chemical Engineering, University of Calabria, Via P. Bucci, 44/A, I-87036 Rende (CS), Italy; pietro.argurio@unical.it
* Correspondence: t.marino@itm.cnr.it (T.M.); raffaele.molinari@unical.it (R.M.)

Abstract: Photocatalysis combined with membrane technology could offer an enormous potential for power generation in a renewable and sustainable way. Herein, we describe the one-step hydrogen and oxygen evolution through a photocatalytic membrane reactor. Experimental tests were carried out by means of a two-compartment cell in which a modified Nafion membrane separated the oxygen and hydrogen evolution semi-cells, while iron ions permeating through the membrane acted as a redox mediator. Nanosized Au/TiO$_2$ and Au/CeO$_2$ were employed as suspended photocatalysts for hydrogen and oxygen generation, respectively. The influence of initial Fe^{3+} ion concentration, ranging from 5 to 20 mM, was investigated, and the best results in terms of hydrogen and oxygen evolution were registered by working with 5 mM Fe^{3+}. The positive effect of gold on the overall water splitting was confirmed by comparing the photocatalytic results obtained with the modified/unmodified titania and ceria. Au-loading played a key role for controlling the photocatalytic activity, and the optimal percentage for hydrogen and oxygen generation was 0.25 wt%. Under irradiation with visible light, hydrogen and oxygen were produced in stoichiometric amounts. The crucial role of the couple Fe^{3+}/Fe^{2+} and of the membrane on the performance of the overall photocatalytic system was found.

Keywords: water splitting; Z-scheme; photocatalysis; photocatalytic membrane reactor

1. Introduction

Photocatalytic water splitting to generate hydrogen from solar light is a process that can play an important role for the future development of clean and renewable energies alternative to fossil fuels [1–8]. The combination of photocatalysis, which allows converting solar energy into chemical energy, and membrane-based operations could offer the possibility to achieve one-step hydrogen generation from water splitting at ambient temperature without needing further energy inputs. Hydrogen attracted increasing interest as a valid candidate for fossil-fuel substitution, enough to give rise to create the so-called "hydrogen economy" in 1970 [9–12].

From a thermodynamic point of view, hydrogen oxidation can offer three times the energy per gram in comparison to fossil fuels as gasoline. Moreover, hydrogen oxidation leads to the formation of water, making it a zero-emission fuel. Hydrogen also finds applications in the chemical industry as a reagent in fine-chemical synthesis [12].

Since Fujishima and Honda discovered photocatalytic water splitting by means of TiO_2 electrodes in 1972 [13], noticeable works were carried out in order to investigate photocatalytic-based hydrogen generation from water via both photocatalysis and photoelectrochemistry [14]. Particular attention was paid to semiconductor oxides, due to their simple preparation through calcination and their stability toward oxygen generation [15–19]. The water-splitting pathway involves a series of radical reactions initiated by light-driven photocatalyst activation, as deeply described in the literature [3].

Among the well-known semiconductors, nanosized TiO_2 is attracting more and more interest, due to its unique properties of physico-chemical stability and inertness, low cost, biocompatibility, durability, long-term photo-stability, and potent oxidative power under ultraviolet (UV)-light irradiation [20–22]. Despite its numerous advantages, the use of TiO_2 still presents a limitation, i.e., only UV light, representing ~4% of total solar energy, can be absorbed by titania nanoparticles. Therefore, extending TiO_2 light absorption to the visible fraction represents a challenging target for photocatalysis applications. Various techniques, such as noble-metal and non-metal doping, dye sensitization, and coupling with carbon materials were adopted in order to modify the electronic band of titania [23].

In a previous work, we reported that gold nanoparticles supported on titania (Au/TiO_2) represent a suitable photocatalyst for the generation of hydrogen with visible light using methanol and ethylenediaminetetraacetic acid (EDTA) as sacrificial electron donors [14]. A remarkable overall efficiency of approximately 5% measured at 560 nm was determined [14]. In this system, gold nanoparticles act as a durable and stable photosensitizer, absorbing visible light and injecting electrons in the conduction band of the TiO_2. Using 0.25 wt% gold loading on titania and methanol as a sacrificial agent, ~98 µmol of hydrogen was obtained (catalyst content 2 g/L) after 4 h of irradiation with visible light [14].

Also, we showed that ceria of small average particle size can behave as a semiconductor with a remarkably high efficiency for the photocatalytic generation of oxygen from water using Ag^+ or Ce^{3+} as a sacrificial electron acceptor [24]. The best performing CeO_2 sample was that prepared using a biopolymer "alginate" as a templating agent to synthesize about 5 nm of average particle size with a Brunauer-Emmett-Teller (BET) surface area of 93 $m^2 \cdot g^{-1}$ [24]. Also, in this case, visible-light photocatalytic activity was implemented by depositing gold nanoparticles on CeO_2 (Au/CeO_2), which allowed achieving ~50 µmol of oxygen when the aqueous suspension containing 0.25 wt% gold deposited on CeO_2 was irradiated for 4 h with visible light in the presence of $AgNO_3$ as a sacrificial agent [24].

Considering the above precedents and the visible-light photocatalytic activity for independent hydrogen and oxygen generation using Au/TiO_2 or Au/CeO_2, respectively, in the presence of an appropriate sacrificial agent, it occurs that these two photocatalysts could also work in a system to perform the simultaneous generation of hydrogen and oxygen in the absence of sacrificial agents using a Z-scheme [25–28]. In this Z-scheme methodology, hydrogen and oxygen are generated photocatalytically in different cells that are irradiated and separated by a membrane [5,29–34]. An electrolyte is used to ensure the electroneutrality in each cell and to allow charge transfer from one compartment to the other.

Li et al. [5] reported concomitant hydrogen generation and phenol degradation in a photocatalytic twin reactor under simulated solar light. In the proposed system, Pt/STO:Rh was used as a photocatalyst for hydrogen evolution, while WO_3 was chosen for phenol oxidation. A Nafion membrane separated the two compartments of the cell. Fe^{3+}/Fe^{2+} pairs were used for electron transfer. The obtained data evidenced a hydrogen generation rate of 1.90 $µmol \cdot g^{-1} \cdot h^{-1}$. Moreover, by employing a phenol initial concentration of 200 $µmol \cdot L^{-1}$, hydrogen yield reached a value of 11.37 $µmol \cdot g^{-1}$ after 6 h of irradiation, corresponding to an increase of 20% compared to that of pure water splitting. Fujihara et al. [35] studied water splitting in a two-compartment cell using Pt/TiO_2-anatase as a catalyst for hydrogen generation suspended in a Br_2/Br^- aqueous solution and Pt/TiO_2-rutile for simultaneous oxygen evolution in an Fe^{3+}/Fe^{2+} redox couple solution. Yu et al. [33]

also reported the experimentation of a twin reactor for the synchronized formation of hydrogen, through the photocatalytic activity of $BiVO_4$, and oxygen using $Pt/SrTiO_3$:Rh. A Nafion membrane was inserted in the two-side system to assure the separate generation of the two gases. Similarly to the above mentioned works, the Fe^{3+}/Fe^{2+} redox couple was also selected in this case as a redox mediator.

Hydrogen and oxygen in a stoichiometric ratio (2:1) were obtained, with a maximum hydrogen formation rate of 0.65 $\mu mol \cdot g^{-1} \cdot h^{-1}$. Lo et al. [31] investigated the water-splitting process for the one-step H_2 and O_2 generation by means of a membrane twin reactor under visible-light irradiation. $Pt/SrTiO_3$:Rh and WO_3 were designated as hydrogen- and oxygen-evolution semiconductors, respectively. The formation of the two gases reflected their stoichiometric ratio, with an average hydrogen evolution rate equal to 1.59 $\mu mol \cdot g^{-1} \cdot h^{-1}$.

Nafion represents a valid choice as a membrane material, since it is characterized by outstanding chemical and physical resistance [36] and an affinity for iron species. Ramirez et al. [37] investigated the uptake characteristics of different cations (Fe^{3+}, Cu^{2+}, and Ni^{2+}) by Nafion 117, which is commonly used as a separator for different chemical processes. The membrane exhibits its affinity in the order $Fe^{3+} \geq Ni^{2+} \geq Cu^{2+}$, similar to that reported in a previous study [38]. In another study [39], it was reported that a Nafion/Fe membrane was resistant to the attack of the highly oxidative radical •OH ($E° •OH/–OH$ = 1.90 eV vs. normal hydrogen electrode (NHE)) and did not allow leaching of the Fe exchanged on the sulfonic groups within the 3000-h testing period. Kiwi et al. [40] demonstrated that iron compounds supported on a Nafion membrane gave good results in a photo-Fenton water treatment process, where the Fe ions were fixed and remained active in H_2O_2 decomposition.

In the present work, we studied the overall photocatalytic water splitting using Au nanoparticles as a sensitizer of TiO_2 and CeO_2 semiconductors irradiated with visible light in combination, a Nafion film as a membrane separating two cells, and ferric sulfate as the electrolyte. Diffusion tests on the iron-modified Nafion membrane were performed to determine its ability to allow diffusion of iron species. The influence on system performance of initial Fe^{3+} concentration and of Au loading on the O_2 and H_2 evolution photocatalysts was determined. Finally, the photocatalytic activity of the pairs (Au/TiO_2 and Au/CeO_2) for the photocatalytic water splitting through a Z-scheme under visible light was demonstrated.

2. Materials and Methods

TiO_2 (particle size: 20 nm; rutile/anatase: 85:15, 99.9%) was a commercial P25 sample supplied by Degussa. CeO_2 was prepared starting from an aqueous solution of alginate that was flocculated with cerium nitrate followed by calcination as previously reported [24]. Gold nanoparticles were deposited on TiO_2 and CeO_2 via the deposition–precipitation method starting from $AuHCl_4$ and maintaining pH = 10 as described in Reference [14]. TEM images were recorded with a Jeol 200 Cx microscope operating at 200 kV.

2.1. Photocataytic Tests

The photocatalytic membrane reactors (PMRs) experimented in the present work for simultaneous generation of hydrogen and oxygen from water splitting mimic the Z-scheme mechanism used by plants for natural photosynthesis. The Z-scheme (Figure 1a) basically includes two photocatalysts: (i) the oxygen evolution photocatalyst (Au/CeO_2 in this study) leading to O_2 formation via water oxidation, and (ii) the hydrogen evolution photocatalyst (Au/TiO_2 in this study) which promotes H_2 formation via water reduction. The aqueous suspensions containing the two photocatalysts need to be separated by a membrane able to transports electrons via a redox couple (Fe^{3+}/Fe^{2+} in this study) acting as an electron redox mediator.

The experimental set-up (Figure 1b) consisted of a two-compartment Pyrex cell, each with a volume of 50 mL, separated by a Nafion modified membrane with an exposed membrane surface area of 3.14 cm^2. Each compartment, containing 60 mg of photocatalyst suspended in 30 mL of Milli-Q water (corresponding to 2 $g \cdot L^{-1}$ photocatalyst concentration), was irradiated with a 125-W

medium-pressure mercury lamp (DLU, HDLM E27) equipped with a Pyrex glass jacket which allows maintaining the system at a temperature of 20 °C. The suspensions were purged with argon flow for at least 30 min before irradiation in order to remove dissolved air. For polychromatic visible-light irradiation, an $Fe_2(SO_4)_3$ solution (3% w/v), circulated into the Pyrex glass jacket of the lamp, was used as a cut-off filter ($\lambda > 400$ nm). Hydrogen and oxygen generation was determined by injecting 0.1 mL of each Pyrex cell headspace gas in a gas chromatograph (GC; Agilent 7890A) equipped with a thermal conductivity detector. The GC determination was carried out by operating in isothermal conditions (50 °C), with a capillary column (CP-PoraPLOT Q, molecular sieve, 530 μm inner diameter, 15 m length) and argon as a carrier gas.
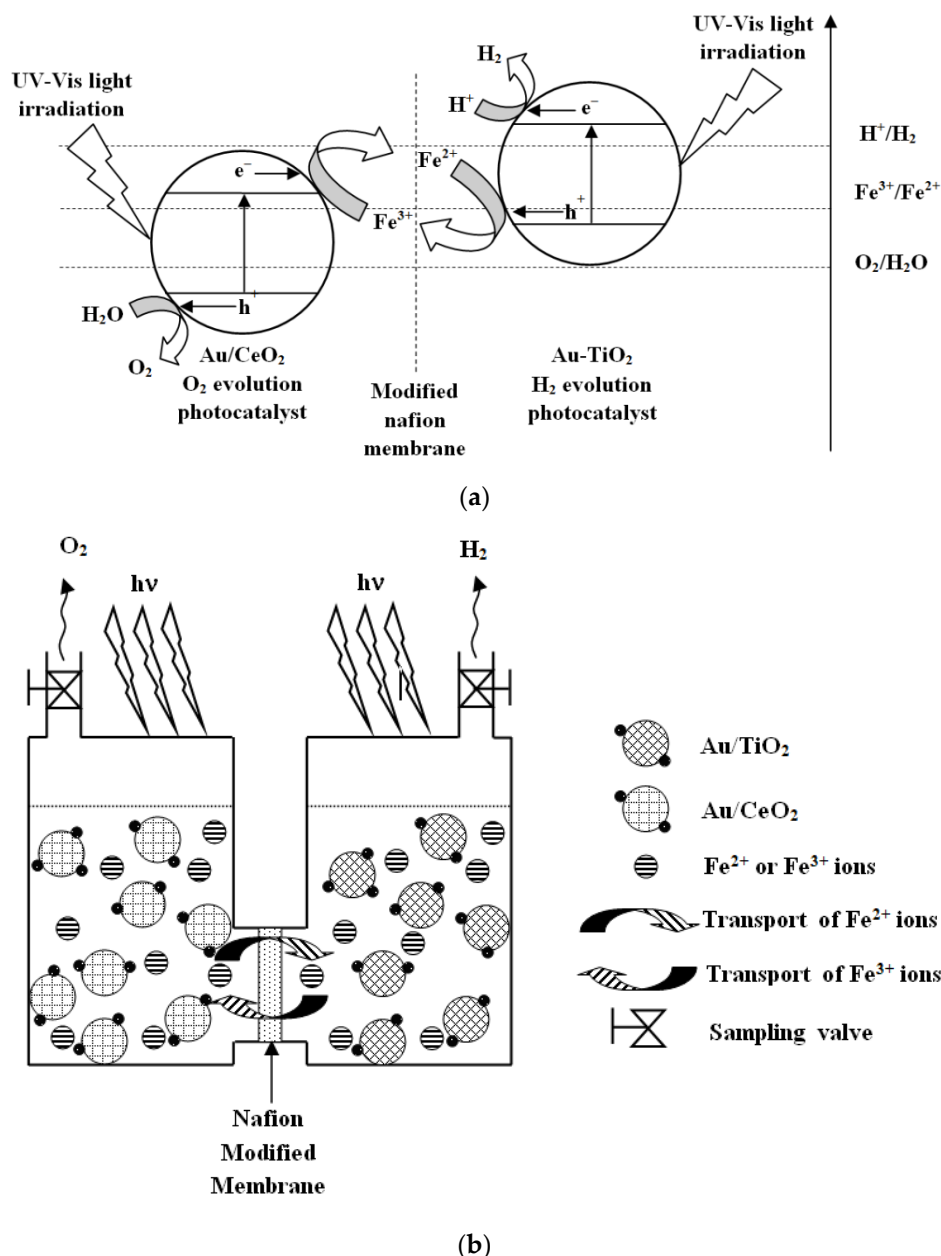

(a)

(b)

Figure 1. (a) Diagram of the Z-scheme overall water splitting using Au/CeO_2 as a photocatalyst for oxygen generation, Au/TiO_2 for hydrogen generation, and Fe^{3+}/Fe^{2+} as a redox couple. **(b)** Conceptual scheme of the set-up used for photocatalytic experiments.

2.2. Membrane Modification

The Nafion 117 membrane (Aldrich, thickness of 178 µm) was modified using the procedure described herein before its use. In the first step, the membrane was boiled in a 1 M HNO_3 solution for 2 h to remove any contaminant; then, it was washed with Milli-Q water, immersed in a 1 M NaOH solution, and subsequently in a 1 M H_2SO_4 solution for 4 h, each for conditioning the membrane [41]. Finally, the Nafion membrane was immersed in a 0.5 M $Fe_2(SO_4)_3$ solution for 24 h to change its functional groups (H^+) with Fe^{3+} ions.

2.3. Iron Spectrophotometric Determination

Spectrophotometric analyses were performed using 1,10-phenanthroline (Fluka, Aquanal Plus kit) and potassium thiocyanate (Aldrich), for total iron ($\lambda = 510$ nm) and ferric ion ($\lambda = 477$ nm) determinations, respectively. Ferrous iron ion concentration present in solution was calculated by the difference between total and ferric iron concentration.

3. Results and Discussion

3.1. Diffusion Test

The iron-containing modified Nafion membrane was tested to determine its ability to allow diffusion of iron species. Similar concentrations of Fe^{2+} and Fe^{3+} as that utilized in the photocatalytic experiments were used in one compartment and, then, the presence of corresponding iron species over time was determined in the other compartment. The corresponding profiles of iron species diffusing through the membrane are provided in Figure 2.
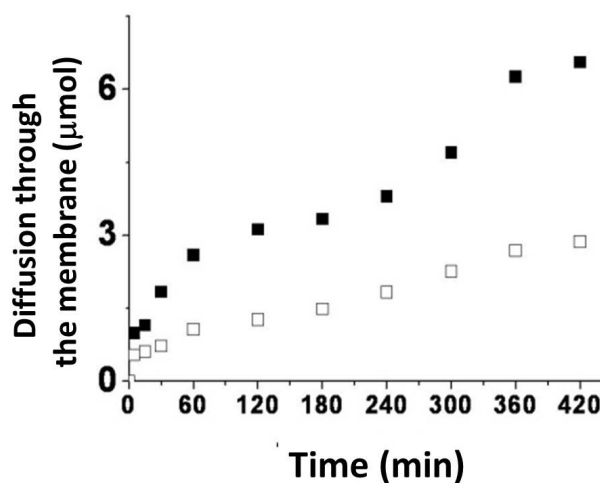

Figure 2. Fe^{2+} (■) and Fe^{3+} (□) transport over time through the Nafion membrane in the compartment cell with no initial salt.

It was observed that, while Fe^{3+} diffusion could be fitted by a straight line, i.e., the concentration of Fe^{3+} in the chamber without it grew linearly over time, similar experiments with Fe^{2+} salt clearly revealed two regimes. These results might be explained considering that, in the first regime, ion exchange of Fe^{3+} and Fe^{2+} occurred in the Nafion membrane concomitantly to the diffusion. In the second regime, the Nafion membrane behaved essentially as a Fe^{2+} exchanger.

The iron content in the membrane before and after its use was estimated by SEM energy dispersive X-ray spectroscopy (EDX) analysis. The results showed an iron weight loading of ~1.3% and this value did not change after using the membrane (Figure 3).
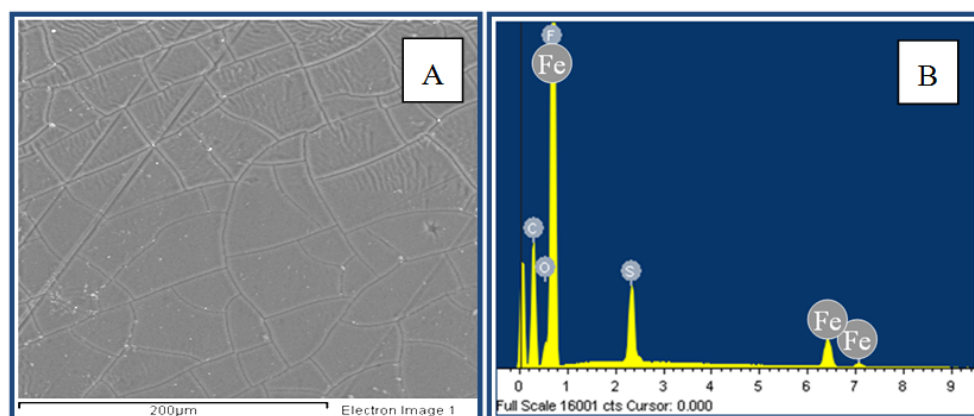
Figure 3. SEM picture of Nafion membrane used for the photocatalytic test (**A**) and energy-dispersive X-ray spectroscopy (EDX) analysis of ferric ion-modified membrane (**B**).

Figure 4 reports TEM pictures of the Au/TiO_2 and Au/CeO_2 photocatalysts. The average particle size of photocatalyst nanoparticles, determined by considering a statistically relevant number of particles in the TEM images of the samples, resulted in 2.7 and 5.0 nm for Au/TiO_2 and Au/CeO_2, respectively.
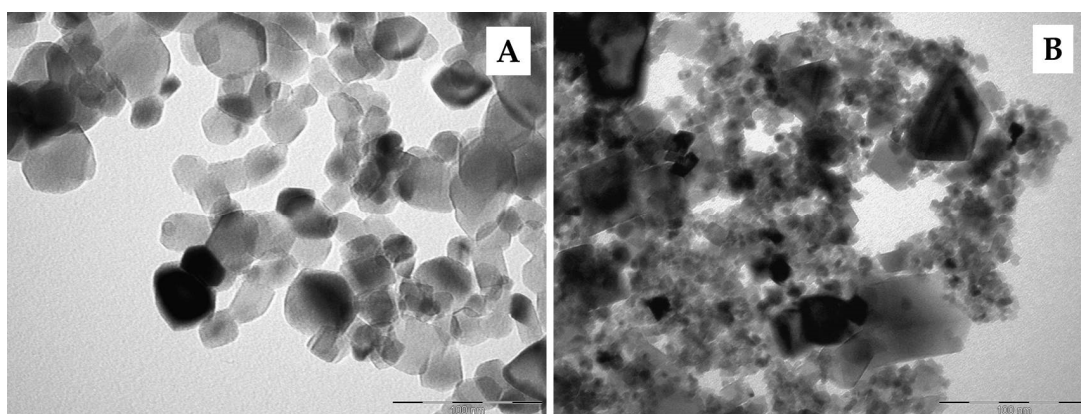

Figure 4. TEM images of Au/TiO_2 (**A**) and Au/CeO_2 (**B**).

3.2. Photocatalytic Tests

For the irradiation of the suspensions, a 125-W medium-pressure mercury lamp was used. This lamp exhibited emission peaks at a discrete wavelength, mostly in the visible region (total irradiation 2133 mW/m^2 with 61% in the visible range). The inset of Figure 5 shows the emission peaks in the spectrum of the lamp used.

Preliminary photocatalytic tests were carried out evidencing the crucial role of the couple Fe^{3+}/Fe^{2+} on both hydrogen and oxygen generation. Indeed, by starting the working of the cell with Fe^{2+} ions in the cell containing Au/TiO_2 and Fe^{3+} ions in the cell containing Au/CeO_2, oxygen generation in both cells was observed during the first 30 min. We suggest that the reason why oxygen was generated in Au/TiO_2 cell instead of the expected hydrogen was because Fe^{3+} was formed by Fe^{2+} oxidation, in the presence of oxygen by air, during the preparation of the work-up cell. Analysis of the Fe^{3+} concentration in the Au/TiO_2 cell confirmed that about 22% of Fe^{2+} ions were oxidized to Fe^{3+} during this stage. The formed Fe^{3+} quenched the generation of hydrogen and promoted the formation of oxygen, owing to the preferential reduction of Fe^{3+} by photogenerated electrons with respect to the photoreduction of water. As a consequence, during the first 30 min, oxygen generation (instead of hydrogen) was observed into the Au/TiO_2 cell before changing to continuous hydrogen generation.

On the basis of these preliminary results, to avoid the presence of Fe^{3+} ions in the Au/TiO_2 cell, the iron ions were initially added to the system only in the form of Fe^{3+} at different concentrations, as reported in Table 1, in the cell containing Au/CeO_2, while, in the Au/TiO_2 cell, the initial iron concentration was zero. Figure 5 shows the temporal evolution of hydrogen in the Au (0.25 wt%)/TiO_2 cell and oxygen in the Au (0.25 wt%)/CeO_2 cell when 5 mM Fe^{3+} was added in the Au/CeO_2 cell. Operating under these conditions, the reaction started on Au/CeO_2 with oxygen evolution via water oxidation coupled with the reduction of Fe^{3+} to Fe^{2+}. The so-produced Fe^{2+} ions permeated across the Nafion modified membrane starting hydrogen evolution in the Au/TiO_2 compartment. As a consequence, during this early stage of the reaction (approximately 5 min), the ratio H_2:O_2 was about 1:1 (see Figure 5) and evidenced that H_2 generation was promoted by Fe^{2+} which permeated through the membrane. After this initial stage, two regimes can be observed: a first one, until 60 min, and a second one, from 60 to 300 min. This trend can be explained considering that, in Figure 2, a similar trend with the same two regimes can be observed for Fe^{2+} permeation through the membrane. It could be deduced that Fe^{2+} ion diffusion during the first regime was faster than that during the second regime (0.043 vs. 0.022 μmol_{Fe}^{2+} min^{-1}) and this behavior affected the photocatalytic reaction. Indeed, the Fe^{2+} ions produced in the Au/CeO_2 cell permeated across the membrane and promoted a generation of hydrogen in the Au/TiO_2 cell. After 300 min, a very low hydrogen production was detected, probably because of the negligible permeation of Fe^{2+} ions across the membrane (see Figure 2) which blocked the Z-scheme mechanism. However, it should be observed that both photocatalysts efficiently worked during these two regimes (slopes of 1.25 $\mu mol_{H2} \cdot min^{-1}$ during the first regime and 0.41 $\mu mol_{H2} \cdot min^{-1}$ during the second regime), promoting the simultaneous generation of hydrogen and oxygen in a stoichiometric amount in the Au/TiO_2 and Au/CeO_2 cells, respectively, and that blocking was only caused by Fe^{2+} ion permeation through the membrane.
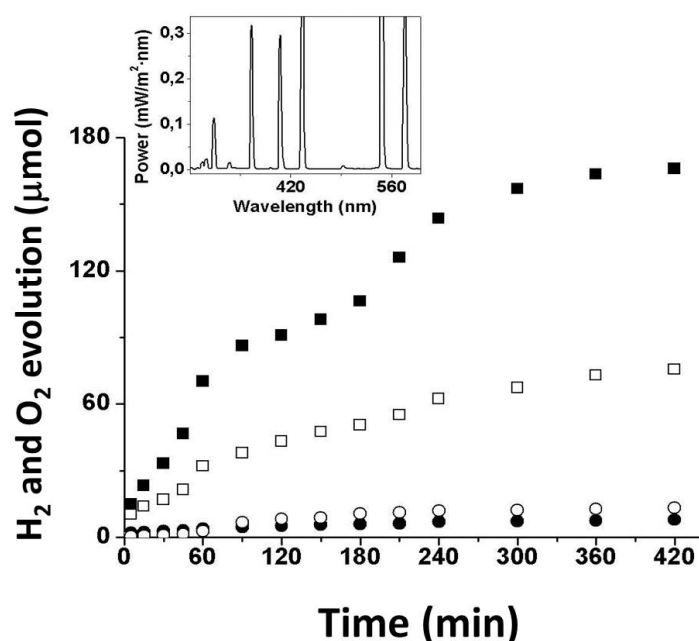

Figure 5. Hydrogen production (■) using Au (0.25 wt%)/TiO_2 and oxygen production (□) using Au (0.25 wt%)/CeO_2 compared with hydrogen production (●) using TiO_2 and oxygen production (○) using CeO_2 only (initial Fe^{3+} concentration was 5 mM in the Au/CeO_2 cell and initial Fe^{2+} concentration was zero in the Au/TiO_2 cell).

The initial concentration of Fe^{3+} ions in the Au/CeO_2 cell varied in the range from 2 to 50 mM, and it was found that 5 mM gave the best photocatalytic performance with the highest initial reaction rate (Table 1).

Table 1. Photocatalytic activity (initial reaction rate, r_0, evolved hydrogen and oxygen at 7 h) of the series of ferric aqueous solutions (initial Fe^{3+} concentration, C_0) under study, using Au (0.25 wt%)/TiO$_2$ and Au (0.25 wt%)/CeO$_2$ for hydrogen and oxygen generation, respectively.

C_0 Fe^{3+} (mM)	Evolved H$_{2,7h}$ (μmol)	Evolved O$_{2,7h}$ (μmol)	H$_2$ $r_0 \times 10^2$ (μmol·min^{-1})	O$_2$ $r_0 \times 10^2$ (μmol·min^{-1})
2	56.2	28.1	34.2	20.7
5	166.1	75.6	114.0	53.4
10	86.2	43.0	96.3	32.5
20	43.2	24.2	34.8	21.1
50	25.5	16.3	33.4	23.5

Au/CeO$_2$ was selective for oxygen generation as it was found to be unable to generate hydrogen. The reason for this behavior might be related to the energy of the electrons in the conduction band of Au/CeO$_2$, which was not sufficient for water reduction (see Figure 1). In contrast, these electrons were able to reduce Fe^{3+} to Fe^{2+}.

The influence of gold on the photocatalytic performance of the Z-scheme overall water splitting by TiO$_2$ and CeO$_2$ was determined by comparing the photocatalytic activity of the gold-containing semiconductors in comparison with the same semiconductors without gold (Figure 5).

As expected, despite the irradiation source used not permitting exclusively visible-light emission, a positive effect of the presence of gold was observed.

The gold loading plays an important role in the photocatalytic efficiency of the system. To demonstrate this point, we performed some photocatalytic tests with equal gold loading on titania and ceria varying from 0.25 to 1.0 wt%. By measuring the initial rate of hydrogen generation, it was concluded that the optimum gold loading under these conditions was the lowest (0.25 wt%) (Table 2).

Table 2. Photocatalytic activity (initial reaction rate, r_0, evolved hydrogen and oxygen at 7 h) of the series of gold-containing samples under study, using a 5 mM ferric solution and TiO$_2$ and CeO$_2$ as photocatalysts for hydrogen and oxygen generation, respectively.

Au Loading (wt%)	Evolved H$_{2,7h}$ (μmol)	Evolved O$_{2,7h}$ (μmol)	H$_2$ $r_0 \times 10^2$ (μmol·min^{-1})	O$_2$ $r_0 \times 10^2$ (μmol·min^{-1})
0.25	166.1	75.6	114.0	53.4
0.6	152.0	61.3	112.1	70.8
1.0	71.0	25.1	67.0	32.2

Au content in the aqueous reacting environment after the reaction was below the detection limit (0.1 ppm).

In a precedent work it was also observed that Au loading is a key parameter controlling the photocatalytic activity of Au/TiO$_2$ and that an optimal Au percentage exists. Since the presence of Au nanoparticles is detrimental for the efficiency of TiO$_2$ photocatalysis under UV irradiation, but enhances the photocatalytic efficiency for visible-light irradiation, the observed beneficial effect of Au might be explained considering that, by operating under our conditions, visible light gave the largest contribution to the total photocatalytic water splitting. In view of the above data, we propose the water-splitting mechanism shown in Figure 6.

Upon light absorption (mostly visible), electrons (in the conduction band) and holes (in the valence band) were generated in Au/CeO$_2$. It was found that electrons in Au/CeO$_2$ were inefficient to generate hydrogen and, therefore, they were captured by Fe^{3+}, forming Fe^{2+} ions that diffused through the Nafion membrane to the Au/TiO$_2$ cell. The holes located on Au of the Au/CeO$_2$ photocatalyst had sufficient oxidation power to generate oxygen via water oxidation as previously proven [42]. In the Au/TiO$_2$ cell, similar charge separation as in the Au/CeO$_2$ cell would occur upon photon absorption; however, in this case, the reduction potential of the TiO$_2$ conduction band had enough energy to form

hydrogen via water reduction. The holes on Au were, in this case, quenched by oxidation of Fe^{2+} diffusing through the Nafion membrane from the Au/CeO_2 cell.
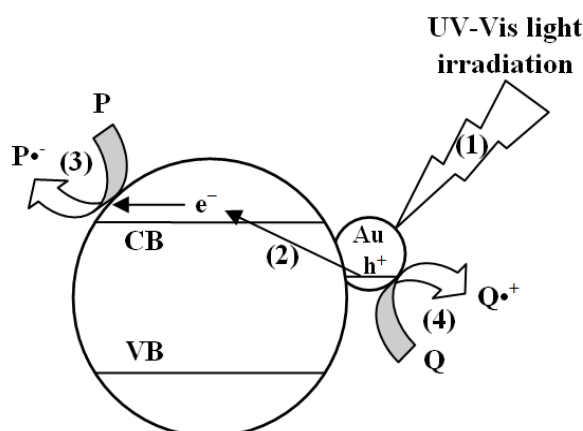

Figure 6. Elementary steps occurring in the photocatalytic reaction upon irradiation of a gold-containing photocatalyst sample under ultraviolet (UV) irradiation: (1) photon absorption; (2) electron migration from Au to semiconductor conduction band; (3) electron quenching by P; (4) Q oxidation by H^+ mediated by Au.

To demonstrate the photocatalytic activity of the pair Au/TiO_2 and Au/CeO_2 for the overall water splitting through a Z-scheme under visible light, analogous photocatalytic experiments were performed by filtering light to almost completely remove the irradiation wavelength below 400 nm (Figure 7). Under these conditions, the irradiance decreased from 2133 $mW \cdot m^{-2}$ to 570 $mW \cdot m^{-2}$. In Figure 7, the two regimes previously observed in Figure 5 were not present. This can be ascribed to the lower irradiance (3.6 times lower for the visible light compared to UV irradiation), which decreased the H_2/O_2 generation rate (slopes of 0.08 $\mu mol_{H2} \cdot min^{-1}$ and 0.04 $\mu mol_{O2} \cdot min^{-1}$), thus requiring a lower Fe^{2+} ion diffusion rate.
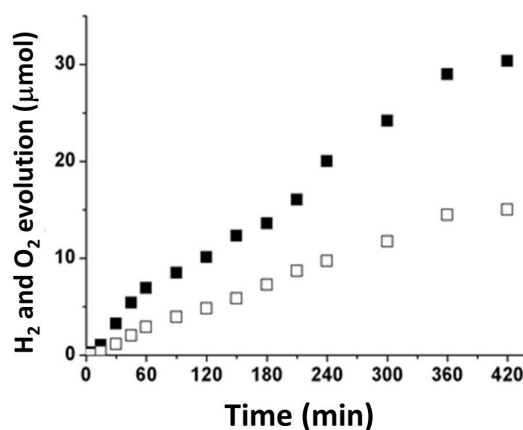

Figure 7. Hydrogen production (■) using Au (0.25 wt%)/TiO_2 and oxygen production (□) using Au (0.25 wt%)/CeO_2, under visible-light irradiation (initial Fe^{3+} concentration was 5 mM in the Au/CeO_2 cell and initial Fe^{2+} concentration was zero in the Au/TiO_2 cell).

Also under these conditions, hydrogen and oxygen generation was observed in stoichiometric amounts in the Au/TiO_2 and Au/CeO_2 cells, respectively (Table 3).

Table 3. Photocatalytic activity (initial reaction rate, r_0, evolved hydrogen and oxygen at 7 h) of the Au (0.25 wt%)/TiO_2 and Au (0.25 wt%)/CeO_2 samples using a 5 mM ferric solution for hydrogen and oxygen generation, respectively, under visible-light irradiation.

Au Loading (wt%)	Evolved $H_{2,7h}$ (μmol)	Evolved $O_{2,7h}$ (μmol)	H_2 $r_0 \times 10^2$ (μmol·min^{-1})	O_2 $r_0 \times 10^2$ (μmol·min^{-1})
0.25	30.36	14.89	11.0	4.2

4. Conclusions

In the present article, we combined the high activity of Au/TiO_2 to photocatalytically generate hydrogen with the high activity of Au/CeO_2 to promote oxygen evolution from water. Thus, overall water splitting was obtained by operating through a Z-scheme using a Nafion membrane and Fe^{3+}/Fe^{2+} as an electrolyte.

The obtained results showed the following:

— The employed photocatalysts promoted simultaneous hydrogen and oxygen generation;
— The optimal content of ferric ions in the Au/CeO_2 compartment was 5 mM;
— Gold operated as a photosensitizer allowing photocatalytic hydrogen and oxygen formation under visible light;
— A gold loading of 0.25 wt% led to the best results in terms of hydrogen and oxygen evolution (166.1 and 75.6 μmol, respectively, after 7 h of UV-visible-light irradiation);
— Hydrogen and oxygen were produced in stoichiometric amounts, i.e., 30.36 and 14.89 μmol, respectively, after 7 h of irradiation with visible light;
— The decrease in permeation rate of iron ions through the Nafion membrane affected the photocatalytic performance, slowing the generation rates of both hydrogen and oxygen.

References

1. Bamwenda, G.R.; Tsubota, S.; Nakamura, T.; Haruta, M. Photoassisted Hydrogen-Production from a water-ethanol solution—A Comparison of activities of Au-TiO_2 and Pt-TiO_2. *J. Photochem. Photobiol. A-Chem.* **1995**, *89*, 177–189. [CrossRef]
2. Khan, S.U.M.; Al-Shahry, M.; Ingler, W.B. Efficient photochemical water splitting by a chemically modified n-TiO_2. *Science* **2002**, *297*, 2243–2245. [CrossRef] [PubMed]
3. Loddo, V.; Palmisano, L.; Marino, T.; Molinari, R. Membranes for photocatalysis in water and wastewater treatment. In *Advanced Membrane Science and Technology for Sustainable Energy and Environmental Applications*; Basile, A., Nunes, S.P., Eds.; Woodhead Publishing: Sawston, UK, 2011; pp. 746–768.
4. Maeda, K.; Domen, K. New non-oxide photocatalysts designed for overall water splitting under visible light. *J. Phys. Chem. C* **2007**, *111*, 7851–7861. [CrossRef]
5. Li, D.; Yu, J.C.; Nguyen, V.; Wu, C.S.; Wang, X. A dual-function photocatalytic system for simultaneous separating hydrogen from water splitting and photocatalytic degradation of phenol in a twin-reactor. *Appl. Catal. B Environ.* **2018**, *239*, 268–279. [CrossRef]
6. Argurio, P.; Fontananova, E.; Molinari, R.; Drioli, E. Photocatalytic Membranes in Photocatalytic Membrane Reactors. *Processes* **2018**, *6*, 162. [CrossRef]
7. Iglesias, O.; Rivero, M.J.; Urtiaga, A.M.; Ortiz, I. Membrane-based photocatalytic systems for process intensification. *Chem. Eng. J.* **2016**, *305*, 136–148. [CrossRef]

8.　Rahimpour, M.R.; Mahmoodi, L. *Performance of Reactors With PMs*; Elsevier Inc.: Amsterdam, The Netherlands, 2018; ISBN 9780128135495.

9.　Molino, A.; Migliori, M.; Blasi, A.; Davoli, M.; Marino, T.; Chianese, S.; Catizzone, E.; Giordano, G. Municipal waste leachate conversion via catalytic supercritical water gasification process. *Fuel* **2017**, *206*, 155–161. [CrossRef]

10.　Marbán, G.; Valdés-Solís, T. Towards the hydrogen economy? *Int. J. Hydrog. Energy* **2007**, *32*, 1625–1637. [CrossRef]

11.　Armaroli, N.; Balzani, V. The hydrogen issue. *ChemSusChem* **2011**, *4*, 21–36. [CrossRef]

12.　Ball, M.; Wietschel, M. The future of hydrogen—Opportunities and challenges. *Int. J. Hydrog. Energy* **2009**, *34*, 615–627. [CrossRef]

13.　Fujishima, A.; Honda, K. Electrochemical photolysis of water at a semiconductor electrode. *Nature* **1972**, *238*, 37–38. [CrossRef] [PubMed]

14.　Silva, C.G.; Juárez, R.; Marino, T.; Molinari, R.; García, H. Influence of excitation wavelength (UV or visible light) on the photocatalytic activity of titania containing gold nanoparticles for the generation of hydrogen or oxygen from water. *J. Am. Chem. Soc.* **2011**, *133*, 595–602. [CrossRef] [PubMed]

15.　Galiano, F.; Song, X.; Marino, T.; Boerrigter, M.; Saoncella, O.; Simone, S.; Faccini, M.; Chaumette, C.; Drioli, E.; Figoli, A. Novel Photocatalytic PVDF/Nano-TiO$_2$ Hollow Fibers for Environmental Remediation. *Polymers* **2018**, *10*, 1134. [CrossRef]

16.　Molinari, R.; Caruso, A.; Palmisano, L. Photocatalytic Processes in Membrane Reactors. In *Comprehensive Membrane Science and Engineering*; Drioli, E., Giorno, L., Eds.; Elsevier Science B.V.: Oxford, UK, 2010; Volume 3, pp. 165–193, ISBN 9780080932507.

17.　Hoffmann, M.R.; Martin, S.T.; Choi, W.; Bahnemann, D.W. Environmental Applications of Semiconductor Photocatalysis. *Chem. Rev.* **1995**, *95*, 69–96. [CrossRef]

18.　Schneider, J.; Matsuoka, M.; Takeuchi, M.; Zhang, J.; Horiuchi, Y.; Anpo, M.; Bahnemann, D.W. Understanding TiO$_2$ Photocatalysis: Mechanisms and Materials. *Chem. Rev.* **2014**, *114*, 9919–9986. [CrossRef] [PubMed]

19.　Kudo, A.; Miseki, Y. Heterogeneous photocatalyst materials for water splitting. *Chem. Soc. Rev.* **2009**, *38*, 253–278. [CrossRef] [PubMed]

20.　Marino, T.; Boerigter, M.; Faccini, M.; Chaumette, C.; Arockiasamy, L.; Bundschuh, J.; Figoli, A. Photocatalytic activity and synthesis procedures of TiO$_2$ nanoparticles for potential applications in membranes. In *Application of Nanotechnology in Membranes for Water Treatment*; Hoinkis, J., Figoli, A., Altinkaya, S.A., Bundschuh, J., Eds.; CRC, Taylor and Francis Group: Boca Raton, FL, USA, 2017; ISBN 9781138896581.

21.　Figoli, A.; Marino, T.; Simone, S.; Boerighter, M.; Faccin, M.; Chaumette, C.; Drioli, E. Application of nano-sized TiO$_2$ in membrane technology. In *Application of Nanotechnology in Membranes for Water Treatment*; Hoinkis, J., Figoli, A., Altinkaya, S.A., Bundschuh, J., Eds.; CRC, Taylor and Francis Group: Boca Raton, FL, USA, 2017; ISBN 9781138896581.

22.　Fujishima, A.; Rao, T.N.; Tryk, D.A. Titanium dioxide photocatalysis. *J. Photochem. Photobiol. C Photochem. Rev.* **2000**, *1*, 1–21. [CrossRef]

23.　Kumar, S.G.; Devi, L.G. Review on modified TiO$_2$ photocatalysis under UV/visible light: Selected results and related mechanisms on interfacial charge carrier transfer dynamics. *J. Phys. Chem. A* **2011**, *115*, 13211–13241. [CrossRef]

24.　Primo, A.; Marino, T.; Corma, A.; Molinari, R.; Garcia, H. Efficient visible-light photocatalytic water splitting by minute amounts of gold supported on nanoparticulate CeO$_2$ obtained by a biopolymer templating method. *J. Am. Chem. Soc.* **2011**, *133*, 6930–6933. [CrossRef]

25.　Marino, T.; Primo, A.; Corma, A.; Molinari, R.; Garcia, H. Photocatalytic overall water splitting by combining gold nanoparticles supported on TiO$_2$ and CeO$_2$. In Proceedings of the 2nd European Symposium on Photocatalysis, Bordeaux, France, 19 October 2011; p. 76.

26.　Higashi, M.; Abe, R.; Ishikawa, A.; Takata, T.; Ohtani, B.; Domen, K. Z-scheme Overall Water Splitting on Modified-TaON Photocatalysts under Visible Light ($\lambda < 500$ nm). *Chem. Lett.* **2008**, *37*, 138–139. [CrossRef]

27.　Maeda, K.; Higashi, M.; Lu, D.; Abe, R.; Domen, K. Efficient nonsacrificial water splitting through two-step photoexcitation by visible light using a modified oxynitride as a hydrogen evolution photocatalyst. *J. Am. Chem. Soc.* **2010**, *132*, 5858–5868. [CrossRef] [PubMed]

28. Chiarello, G.L.; Tealdi, C.; Mustarelli, P.; Selli, E. Fabrication of Pt/Ti/TiO$_2$ Photoelectrodes by RF-Magnetron Sputtering for Separate Hydrogen and Oxygen Production. *Materials* **2016**, *9*, 279. [CrossRef] [PubMed]

29. Selli, E.; Chiarello, G.L.; Quartarone, E.; Mustarelli, P.; Rossetti, I.; Forni, L. Photocatalytic water splitting device for separate hydrogen and oxygen evolution. *Chem. Commun.* **2007**, *47*, 5022–5024. [CrossRef] [PubMed]

30. Xu, Q.; Zhang, L.; Yu, J.; Wageh, S.; Al-ghamdi, A.A.; Jaroniec, M. Direct Z-scheme photocatalysts: Principles, synthesis, and applications. *Mater. Today* **2018**, *21*, 1042–1063. [CrossRef]

31. Lo, C.; Huang, C.; Liao, C.; Wu, J.C.S. Novel twin reactor for separate evolution of hydrogen and oxygen in photocatalytic water splitting. *Int. J. Hydrog. Energy* **2010**, *35*, 1523–1529. [CrossRef]

32. Seger, B.; Kamat, P.V. Fuel cell geared in reverse: Photocatalytic hydrogen production using a TiO$_2$/Nafion/Pt membrane assembly with no applied bias. *J. Phys. Chem. C* **2009**, *113*, 18946–18952. [CrossRef]

33. Yu, S.-C.; Huang, C.-W.; Liao, C.-H.; Wu, J.C.S.; Chang, S.-T.; Chen, K.-H. A novel membrane reactor for separating hydrogen and oxygen in photocatalytic water splitting. *J. Membr. Sci.* **2011**, *382*, 291–299. [CrossRef]

34. Kitano, M.; Tsujimaru, K.; Anpo, M. Decomposition of water in the separate evolution of hydrogen and oxygen using visible light-responsive TiO$_2$ thin film photocatalysts: Effect of the work function of the substrates on the yield of the reaction. *Appl. Catal. A Gen.* **2006**, *314*, 179–183. [CrossRef]

35. Fujihara, K.; Ohno, T.; Matsumura, M. Splitting of water by electrochemical combination of two photocatalytic reactions on TiO$_2$ particles. *J. Chem. Soc. Faraday Trans.* **1998**, *94*, 3705–3709. [CrossRef]

36. Kraytsberg, A.; Yair, E.-E. Review of Advanced Materials for Proton Exchange Membrane Fuel Cells. *Energy Fuels* **2014**, *28*, 7303–7330. [CrossRef]

37. Ramírez, J.; Godínez, L.A.; Méndez, M.; Meas, Y.; Rodriguez, F.J. Heterogeneous photo-electro-Fenton process using different iron supporting materials. *J. Appl. Electrochem.* **2010**, *40*, 1729–1736. [CrossRef]

38. Feng, J.; Hu, X.; Yue, P.L.; Zhu, H.Y.; Lu, G.Q. Discoloration and mineralization of Reactive Red HE-3B by heterogeneous photo-Fenton reaction. *Water Res.* **2003**, *37*, 3776–3784. [CrossRef]

39. Sabhi, S.; Kiwi, J. Degradation of 2,4-dichlorophenol by immobilized iron catalysts. *Water Res.* **2001**, *35*, 1994–2002. [CrossRef]

40. Kiwi, J. Innovative immobilized Fenton systems useful in the abatement of industrial pollutants. In Proceedings of the Third Asia-Pacific Conference on Sustainable Energy and Environmental Technologies, Hong Kong, China, 3–6 December 2000; p. 562.

41. Goswami, A.K.; Acharya, A.; Pandey, A.K. Study of self-diffusion of monovalent and divalent cations in Nafion-117 ion-exchange membrane. *J. Phys. Chem. B* **2001**. [CrossRef]

42. Silva, C.G.; Bouizi, Y.; Fornés, V.; Garcia, H. Layered Double Hydroxides as Highly Efficient Photocatalysts for Visible Light Oxygen Generation from Water. *J. Am. Chem. Soc.* **2009**, *131*, 13833–13839. [CrossRef] [PubMed]